Journal of Computational Applied Mechanics 2025, 56(1): 87-100

DOI: 10.22059/jcamech.2024.377583.1118

RESEARCH PAPER

Unsteady flow of Casson nano-blood through uneven/composite stenosis porous artery with an inclined magnetic field

I. El Glili [a, *], A. Saidi [a], Y. Foukhari [a], M. Driouich [a], M. Sammouda [a] and K. Gueraoui [b]

[a] *Laboratory of Research in Physics and Engineering Sciences (LRPSI), Polydisciplinary faculty, Sultan Moulay Slimane University, Beni Mellal, Morocco*

[b] *Department of mechanical engineering, University of Ottawa, Ottawa, Canada*

Abstract

Studying the flow of blood through unhealthy arteries has emerged as an important area of focus in recent years. Narrowing of the arteries (stenosis) is the most prevalent types of arterial diseases. The present work aims to explore the impact of an inclined magnetic field on the flow of blood via a stenotic porous artery with gold nanoparticles. The blood is supposed to be non-Newtonian and described utilizing the Casson model. To account for the effect of magneto-hemodynamic, a uniform inclined magnetic field is subjected to the flow of blood. A method of finite difference has been used to solve the equations governing the fluid flow with the boundary conditions. Features hemodynamic variables like as velocity, temperature, wall shear stress, flow rate and impedance resistance are determined at the stenosis's critical height for both composite and irregular stenosis. The present model has been verified by comparing it to previous work, and it is shown to be in great concurrence with the prior work.

Keywords: Blood flow, Stenosis artery, MHD, Non-Newtonian fluid, nanofluid;

1. Introduction

In recent years, nanofluids have become a notable advancement in biomedical engineering. Research on the potential uses of nanoparticles in addressing blood flow issues has had a substantial influence on current bio-science publications. Nanomaterials are created using nanoscale methods and may exhibit a range of shapes such as platelet, cylinders, blades, spherical particles, and more. Nanofluids are created by combining nanoparticles with a base fluid that has less effective thermophysical characteristics, resulting in another class of functional fluids. Jiang et al. [1] reported that physiologically suitable copper dosages might effectively cure hypertrophic cardiomyopathy caused by prolonged pressure overload. Nadeem and Ijaz [2] evaluated the influence of slip conditions on the flow of blood via a tapered stenosis artery in the existence of nanoparticles. Nanomaterials were utilized to study the potential of targeted medication delivery in cancer treatment by Bahrami et al. [3].

Based on the World Health Organization, illnesses that are not infectious account for 68% of all deaths, with cardiovascular illness contributing to one-third [4]. Atherosclerosis is the causes of these phenomena, a condition in which plaque accumulates in the arterial lumen, resulting in stenosis, which prevents blood from accessing outlying

* Corresponding author: Issa.elglilifpb@usms.ac.ma

body cells. Most studies looked at the relationship between artery constriction and dynamics of blood flow, treating blood as a Newtonian fluid. At shear rates above 100 s^{-1}, blood in bigger arteries exhibits aggressive Newtonian comportment. It is widely recognized that small-diameter, low-shear arteries display exceptional non-Newtonian blood comportment, since blood is a cells suspension. In modern research, the Casson model is widely used. Casson fluid displays yield stress properties. When the yield stress is sufficiently strong, the Casson fluid turns into a Newtonian fluid. In a study by Walawender et al. [5], pressure drop and volumetric flow rate were experimentally measured to approximate blood using Casson fluid. Presuming blood as Casson fluid passing via a stenosed artery, Sarifuddin et al. [6] employed the Marker and Cell technique to numerically solve the equations. Das et al. [7] used Casson fluid to evaluate blood rheology and explored solute dispersion via a stenotic tube with an absorbent wall. Padma et al. [8] investigated how yield stress influences the electromagnetohydrodynamic motion of Casson fluid as it passes within a mild obstructed inclined tapered artery. Recently, using the Casson fluid model, Gandhi et al. [9] conducted an entropy generation investigation of unsteady flow of blood across an irregular stenosed artery with permeable walls.

According to the above review of literature, no effort has been made to investigate the effect of inclined magnetic field on flow of blood through stenotic artery utilizing the non-Newtonian Casson fluid with gold (Au) nanoparticles. The present work creates a new mathematical model to assess the impacts of Au nanoparticles traveling through a stenotic artery comparing tow shapes composite and irregular stenosis, with body acceleration, viscous dissipation, inclined Magnetic field, and thermal radiation.

2. Mathematical Formulation

2.1. Geometry of the stenosis

The cylindrical coordinate system (r, θ, z) is used to investigate the incompressible flow of blood in the porous stenosis artery. Let the z axis represent the arterial axis, with (θ, r) denoting the circumferential and radial directions, respectively. The form of the stenosis in the arterial portion may be described as follows,

For the composite stenosis [10, 11],

$$R(z)=\begin{cases} a-2\delta(z-d), & d\le z\le d+\dfrac{l_0}{2} \\ a-\left(\dfrac{\delta}{2}\right)\left(1+\cos\left(2\pi\left(z-d-\left(\dfrac{l_0}{2}\right)\right)\right)\right), & d+\dfrac{l_0}{2}\le z\le d+l_0 \\ a. & otherwise \end{cases} \tag{1}$$

For the irregular stenosis [10, 11],

$$R(z)=\begin{cases} a-2\delta\left(\begin{array}{c}\cos\left(2\pi\left(\dfrac{z-d}{2}-\dfrac{l_0}{4}\right)\right)- \\ \left(\dfrac{7}{100}\right)\left(\cos\left(32\pi\left(z-2d-\dfrac{l_0}{2}\right)\right)\right)\end{array}\right), & d\le z\le d+l_0 \\ a. & otherwise \end{cases} \tag{2}$$

In Figure 1, a represents the non-stenosis artery radius, l_0 represents the stenosis length, d represents the non-stenotic area length, and δ indicates the stenosis height. Figure 2 represents the two different shapes of the stenosis considered.

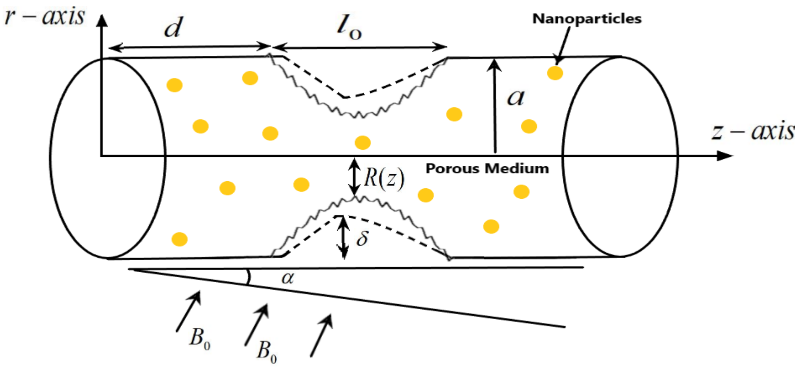

Fig. 1: Geometry of the stenosis artery

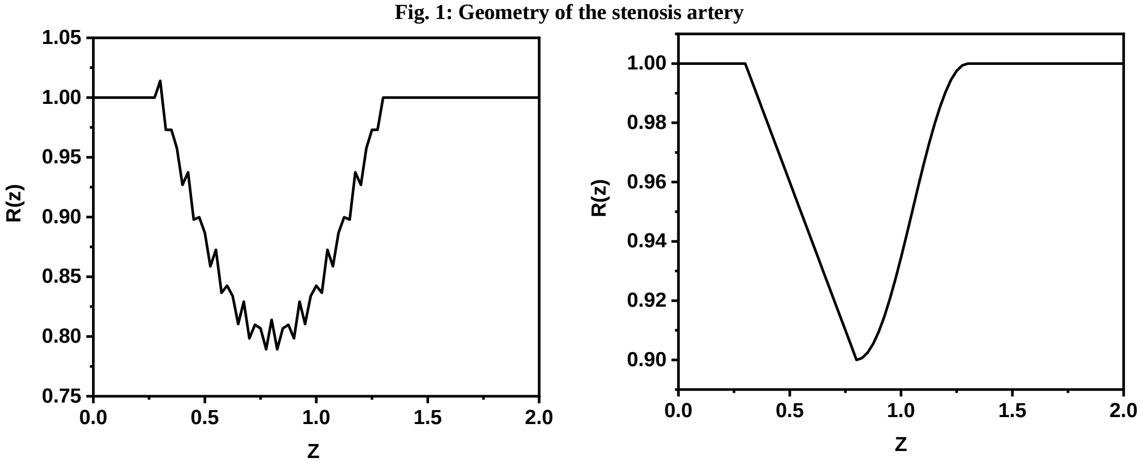

(a) (b)

Fig 2: Representation of the shape of the stenosis (a) Irregular stenosis, (b) Composite stenosis

2.2. Governing equations

Assuming that blood pumping in the artery is unsteady and bidirectional, the velocity and temperature profiles can be described as follows,

$$\vec{V}=\left[U\left(r,z,t\right),0,W\left(r,z,t\right)\right], \tag{3}$$

$$T=T\left(r,z,t\right). \tag{4}$$

In Eq. (3), u and w denote radial and axial velocity components. Thus, continuity, momentum and energy may be expressed using the following conservation equations [12, 13],

$$\frac{\partial\bar{u}}{\partial\bar{r}}+\frac{\bar{u}}{\bar{r}}+\frac{\partial\bar{w}}{\partial\bar{z}}=0, \tag{5}$$

$$\rho_{nf}\left(\frac{\partial\bar{u}}{\partial\bar{t}}+\bar{u}\frac{\partial\bar{u}}{\partial\bar{r}}+\bar{w}\frac{\partial\bar{u}}{\partial\bar{z}}\right)=-\frac{\partial\bar{p}}{\partial\bar{r}}+\left(\frac{1}{\bar{r}}\frac{\partial}{\partial\bar{r}}\left(\bar{r}\bar{S}^{rr}\right)+\frac{\partial}{\partial\bar{z}}\left(\bar{S}^{rz}\right)\right)-\frac{\bar{S}^{\theta\theta}}{\bar{r}}-\frac{\mu_{nf}\bar{u}}{\bar{k}}, \tag{6}$$

$$\rho_{nf}\left(\frac{\partial\bar{w}}{\partial\bar{t}}+\bar{u}\frac{\partial\bar{w}}{\partial\bar{r}}+\bar{w}\frac{\partial\bar{w}}{\partial\bar{z}}\right)=-\frac{\partial\bar{p}}{\partial\bar{z}}+\left(\frac{1}{\bar{r}}\frac{\partial}{\partial\bar{r}}\left(\bar{r}\,\bar{S}^{rz}\right)+\frac{\partial}{\partial\bar{z}}\left(\bar{S}^{zz}\right)\right)+(\rho\gamma)_{nf}\,g(T-T_{w})-\frac{\mu_{nf}\bar{w}}{\bar{k}}-\sigma_{nf}B_{0}^{2}\cos^{2}(\alpha)\,\bar{w}+\rho_{nf}G(t), \tag{7}$$

$$\left(\rho c_{p}\right)_{nf}\left(\frac{\partial\bar{T}}{\partial\bar{t}}+\bar{u}\frac{\partial\bar{T}}{\partial\bar{r}}+\bar{w}\frac{\partial\bar{T}}{\partial\bar{z}}\right)=\bar{S}^{rr}\frac{\partial\bar{u}}{\partial\bar{r}}+\bar{S}^{rz}\left(\frac{\partial\bar{u}}{\partial\bar{z}}+\frac{\partial\bar{w}}{\partial\bar{r}}\right)+\bar{S}^{zz}\frac{\partial\bar{w}}{\partial\bar{z}}+k_{nf}\left(\frac{1}{\bar{r}}\frac{\partial\bar{T}}{\partial\bar{r}}+\frac{\partial^{2}\bar{T}}{\partial\bar{r}^{2}}+\frac{\partial^{2}\bar{T}}{\partial\bar{z}^{2}}\right)-\frac{1}{\bar{r}}\frac{\partial\left(\bar{r}q_{r}\right)}{\partial\bar{r}}. \tag{8}$$

The physical parameters ρ_{nf}, k_{nf}, γ_{nf}, cp_{nf} and μ_{nf} in the above series of equations are, respectively, defined as nanofluid density, thermal conductivity, thermal expansion coefficient, specific heat and dynamic viscosity.

Where q_r represents radiation parameter represented as [14-16],

$$q_r = -\frac{4\sigma^*}{3k^*}\frac{\partial T^4}{\partial r} = -\frac{16\sigma^*}{3k^*}T_0^3\frac{\partial T}{\partial r}. \tag{9}$$

S^{rr}, S^{rz} and S^{zz} components in Eqs. (6)-(8) denote the extra stress component. The rheological equation of Casson model for an incompressible flow [17, 18],

$$S^{ij} = \begin{cases} 2\left(\mu_b + \frac{p_y}{\sqrt{2\pi}}\right)e_{ij} & \pi > \pi_c \\ 2\left(\mu_b + \frac{p_y}{\sqrt{2\pi_c}}\right)e_{ij} & \pi \le \pi_c \end{cases} \tag{10}$$

where $\pi = e_{ij}.e_{ij}$, μ_b, p_y, and π_c is the strain rate product by itself, the non-Newtonian fluid viscosity, the fluid yield stress and a non-Newtonian model critical value, respectively. Eq. (10) has the form below when $\pi \le \pi c$,

$$S^{ij} = 2\mu_b\left(1+\frac{1}{\beta}\right)e_{ij}. \tag{11}$$

Where $\beta = \frac{\mu_b\sqrt{2\pi_c}}{p_y}$, is the Casson fluid parameter.

The boundary condition for the problem,

$$\begin{aligned} &\bar{w}(r,0)=0\,;\bar{T}(r,0)=0 \quad at\ \bar{t}=0 \\ &\frac{\partial\bar{w}}{\partial\bar{r}}=0\,;\frac{\partial\bar{T}}{\partial\bar{r}}=0 \quad at\ \bar{r}=0 \\ &\bar{w}(r,t)=0\,;\bar{T}(r,t)=T_1 \quad at\ \bar{r}=R \end{aligned} \tag{12}$$

2.3. Dimensionless analysis

The dimensionless parameters listed are added to the equations (5)–(8), in order to significantly assist with a numerical solution,

$$\begin{gathered} \bar{r}=R_0 r,\quad \bar{w}=u_0 w,\quad \bar{u}=\frac{\delta^* u_0}{l_0}u,\ \bar{t}=\frac{R_0}{u_0}t,\ \bar{z}=l_0 z,\ \bar{p}=\frac{u_0 l_0\mu_f}{R_0^{\ 2}}p,\ G(t)=\frac{u_0\mu_f}{\rho_f R_0^{\ 2}}\bar{G}(t), \\ \theta=\frac{T-T_1}{T_w-T_1},\ \bar{S}^{rz}=\frac{u_0\mu_f}{R_0}S^{rz},\ \ \bar{S}^{rr}=\frac{u_0\mu_f}{l_0}S^{rr},\ \ \bar{S}^{zz}=\frac{u_0\mu_f}{l_0}S^{zz},\ B_1=\frac{A_0R_0^2}{u_0\mu_f},\ e=\frac{A_1}{A_0} \\ \bar{k}=R_0^{\ 2}k,\ ,\ \ Pr=\frac{(C_p)_f\,\mu_f}{k_f},\ \ Br=\frac{\mu_f u_0^2}{k_f(T_w-T_1)},\mathrm{Re}=\frac{\rho_f u_0 R_0}{\mu_f}, \\ Ma=B_0R_0\sqrt{\frac{\sigma_f}{\mu_f}},Gr=\frac{gR_0^{\ 2}\rho_f\gamma_f(T_w-T_1)}{u_0\mu_f}. \end{gathered} \tag{13}$$

The dimensionless coordinates in this case are, w for axial velocity, u for radial component of velocity, r for radial coordinate, z for axial coordinate, p for pressure and t for time. T_w stands for the wall temperature. Dimensionless geometric parameters are the vascular aspect rate ξ and the parameter of stenosis severity δ. Further non-dimensional numbers are the local thermal Grashof number (Gr), the Reynolds number (Re), the Brinkman number (Br), and the Prandtl number (Pr). After the introduction of the dimensionless parameters of Eq. (13) into Eqs. (5)–(8), the following dimensionless governing equations are obtained:

$$\frac{\rho_{nf}}{\rho_f}\mathrm{Re}\,\delta\xi^2\left(\frac{\partial u}{\partial t}+\delta\xi u\frac{\partial u}{\partial r}+\xi w\frac{\partial u}{\partial z}\right)=-\frac{\partial p}{\partial r}+\xi^2\left(\frac{1}{r}\frac{\partial}{\partial r}\left(r\,S^{rr}\right)+\frac{\partial}{\partial z}\left(S^{rz}\right)\right)+\xi\frac{(\rho\gamma)_{nf}}{(\rho\gamma)_f}\theta-\xi\delta\frac{\mu_{nf}}{\mu_f}\frac{u}{k}, \tag{14}$$

$$\frac{\rho_{nf}}{\rho_f}\mathrm{Re}\left(\frac{\partial w}{\partial t}+\delta\xi u\frac{\partial w}{\partial r}+\xi w\frac{\partial w}{\partial z}\right)=-\frac{\partial p}{\partial z}+\frac{1}{r}\frac{\partial}{\partial r}\left(rS^{rz}\right)+\xi^2\frac{\partial}{\partial z}\left(S^{zz}\right)+\frac{(\rho\gamma)_{nf}}{(\rho\gamma)_f}Gr\,\theta$$
$$-\frac{\mu_{nf}}{\mu_f}\frac{w}{k}-\frac{\sigma_{nf}}{\sigma_f}Ma^2\cos^2(\alpha)w+\frac{\rho_{nf}}{\rho_f}G(t), \tag{15}$$

$$\frac{\left(\rho c_p\right)_{nf}}{\left(\rho c_p\right)_f}\mathrm{Pr}\,\mathrm{Re}\left(\frac{\partial\theta}{\partial t}+\delta\xi u\frac{\partial\theta}{\partial r}+\xi w\frac{\partial\theta}{\partial z}\right)=Br\left(\delta^2\xi^2S^{rr}\frac{\partial u}{\partial r}+S^{rz}\left(\delta\xi^2\frac{\partial u}{\partial z}+\frac{\partial w}{\partial r}\right)+\xi^2S^{zz}\frac{\partial w}{\partial z}\right)$$
$$+\frac{k_{nf}}{k_f}\left(\frac{1}{r}\frac{\partial\theta}{\partial r}+\frac{\partial^2\theta}{\partial r^2}+\xi^2\frac{\partial^2\theta}{\partial z^2}\right)+R_d\left(\frac{1}{r}\frac{\partial\theta}{\partial r}+\frac{\partial^2\theta}{\partial r^2}\right). \tag{16}$$

In addition, the dimensionless form for Eq. (1) and Eq. (2) can be expressed as follows,
For composite stenosis,

$$R(z)=\begin{cases}1-2\delta\left(z-d\right), & d\le z\le d+\frac{1}{2}\\ 1-\left(\frac{\delta}{2}\right)\left(1+\cos\left(2\pi\left(z-2d-\left(\frac{1}{2}\right)\right)\right)\right), & d+\frac{1}{2}\le z\le d\\ 1. & \text{otherwise}\end{cases} \tag{17}$$

For irregular stenosis,

$$R(z)=\begin{cases}1-2\delta\left(\begin{array}{c}\cos\left(2\pi\left(\frac{z-d}{2}-\frac{1}{4}\right)\right)-\\ \left(\frac{7}{100}\right)\left(\cos\left(32\pi\left(z-2d-\frac{1}{2}\right)\right)\right)\end{array}\right), & d<z<d+1\\ 1. & \text{otherwise}\end{cases} \tag{18}$$

A pressure gradient is created throughout the vascular network as a result of the heart pumping blood via the cardiovascular system. Burton [19] states that there are the constant pressure gradient (non-fluctuating) and pulsatile (fluctuating).

$$-\frac{\partial\overline{p}}{\partial\overline{z}}=A_0+A_1\cos\left(\omega_p t\right), \tag{19}$$

where f_1 is the cardiac pulse frequency and $\omega_p = 2\pi f_1$ is the angular frequency. A_0 and A_1 represent the amplitude of the constant and pulsatile pressure gradient components. In a dimensionless form, Eq. (19) can be expressed as,

$$-\frac{\partial p}{\partial z}=B_1\left(1+e\cos\left(\omega_p t\right)\right). \tag{20}$$

A body acceleration G(t) that is given by the following equation affects the blood flow carrying the Au-nanoparticles in the axial direction [10, 20],

$$\overline{G}\left(t\right)=a_0\cos\left(\omega_b t+\alpha\right), \tag{21}$$

where $\omega_b = 2\pi f_2$, f_2 is the acceleration frequency, a_0 is the body's acceleration amplitude and α represents the phase angle.

For the rest of the analysis, two additional assumptions were considered, $\delta \ll 1$ and $\xi=O(1)$, indicating that the stenosis severity is significantly below unity and the artery aspect ratio is approximately equal to unity. Equations (14) - (16) will be clarified to a system of connected differential equations when these presumptions have been applied,

$$\frac{\partial p}{\partial r}=0, \tag{22}$$

$$\begin{aligned}\frac{\rho_{nf}}{\rho_f}\mathrm{Re}\left(\frac{\partial w}{\partial t}\right)&=-\frac{\partial p}{\partial z}+\frac{1}{r}\frac{\partial}{\partial r}\frac{\mu_{nf}}{\mu_f}\left(r\left(1+\frac{1}{\beta}\right)\left(\frac{\partial w}{\partial r}\right)\right)\\&+\frac{(\rho\gamma)_{nf}}{(\rho\gamma)_f}Gr\,\theta-\left(\frac{\mu_{nf}}{\mu_f}\frac{1}{k}+\frac{\sigma_{nf}}{\sigma_f}Ma^2\cos^2(\alpha)\right)w+\frac{\rho_{nf}}{\rho_f}G(t),\end{aligned} \tag{23}$$

$$\frac{(\rho c_p)_{nf}}{(\rho c_p)_f}\mathrm{Pr}\,\mathrm{Re}\left(\frac{\partial \theta}{\partial t}\right)=\frac{\mu_{nf}}{\mu_f}Br\left(1+\frac{1}{\beta}\right)\left(\frac{\partial w}{\partial r}\right)^2+\left(\frac{1}{r}\frac{\partial\theta}{\partial r}+\frac{\partial^2\theta}{\partial r^2}\right)\left(\frac{k_{nf}}{k_f}+R_d\right). \tag{24}$$

The non-dimensional boundary conditions can be written as follows,

$$\begin{aligned}&\left.\frac{\partial w(r,z,t)}{\partial r}\right|_{r=0}=0, \quad w(R,z,t)=0, \quad w(r,z,0)=0,\\&\left.\frac{\partial \theta(r,z,t)}{\partial r}\right|_{r=0}=0, \quad \theta(R,z,t)=1, \quad \theta(r,z,0)=0.\end{aligned} \tag{25}$$

2.4. Radial coordinate transformation

After a dimensionalities and simplification of the governing equation a transformation of radial coordinate is utilized to convert the geometry in a rectangular domain by employing $x={}^{r}\!/_{R}$, the equations take the form,

$$\frac{\rho_{nf}}{\rho_f}\mathrm{Re}\frac{\partial w}{\partial t}=B_1\left(1+e\cos(\omega_p t)\right)+\frac{1}{R^2}\left(1+\frac{1}{\beta}\right)\frac{\mu_{nf}}{\mu_f}\left(\frac{\partial^2 w}{\partial x^2}+\frac{1}{x}\frac{\partial w}{\partial x}\right)+\frac{(\rho\gamma)_{nf}}{(\rho\gamma)_f}Gr\,\theta-\left(\frac{\sigma_{nf}}{\sigma_f}Ma^2\cos^2(\alpha)+\frac{\mu_{nf}}{\mu_f}\frac{1}{k}\right)w+\frac{\rho_{nf}}{\rho_f}G(t), \tag{26}$$

$$\frac{(\rho c_p)_{nf}}{(\rho c_p)_f}\mathrm{Re}\,\mathrm{Pr}\frac{\partial\theta}{\partial t}=\frac{Br}{R^2}\frac{\mu_{nf}}{\mu_f}\left(1+\frac{1}{\beta}\right)\left(\frac{\partial w}{\partial x}\right)^2+\frac{1}{R^2}\left[\frac{\partial^2\theta}{\partial x^2}+\frac{1}{x}\frac{\partial\theta}{\partial x}\right]\left(\frac{k_{nf}}{k_f}+R_d\right). \tag{27}$$

The associated boundary conditions,

$$\begin{aligned}&w|_{t=0}=0\ ,\ \ \theta|_{t=0}=0\ ,\\&\left.\frac{\partial w}{\partial x}\right|_{x=0}=0,\ w|_{x=1}=0\ ,\ \left.\frac{\partial\theta}{\partial x}\right|_{x=0}=0,\ \ \theta|_{x=1}=1.\end{aligned} \tag{28}$$

The flow resistance expression, the flow rate and wall shear stress take the form respectively,

$$\Lambda=\frac{\left|L\left(\frac{\partial p}{\partial z}\right)\right|}{Q_f}, \tag{29}$$

$$Q_f=2\pi R^2\int_0^1 xw\,dx, \tag{30}$$

$$S^{rz}=-\frac{1}{R}\left(1+\frac{1}{\beta}\right)\left.\left(\frac{\partial w}{\partial x}\right)\right|_{x=1}. \tag{31}$$

The following are the thermo-physical characteristics of nanofluid [21-23],

$$\mu_{nf} = \frac{\mu_f}{(1-\phi)^{2.5}}, \quad \alpha_{nf} = \frac{k_{nf}}{(\rho Cp)_{nf}}, \quad \rho_{nf} = (1-\phi)\rho_f + \phi\rho_s$$
$$(\rho Cp)_{nf} = (1-\phi)(\rho Cp)_f + \phi(\rho Cp)_s, \quad (\rho\gamma)_{nf} = (1-\phi)(\rho\gamma)_f + \phi(\rho\gamma)_s, \tag{32}$$
$$\frac{k_{nf}}{k_f} = \frac{k_s + 2k_f - 2\phi(k_f - k_s)}{k_s + 2k_f + \phi(k_f - k_s)}, \quad \frac{\sigma_{nf}}{\sigma_f} = \frac{\sigma_s + 2\sigma_f - 2\phi(\sigma_f - \sigma_s)}{\sigma_s + 2\sigma_f + \phi(\sigma_f - \sigma_s)}.$$

3. Numerical method

There are many numerical methods used to solve partial differential equations, see [24-28]. Analytical or numerical methods are generally the two approaches that may be utilized to address the blood flow problem in a stenosed artery [29-31]. However, applying the analytical solution of such problems to non-Newtonian fluids is challenging. We have decided to use the finite difference approach as a consequence. The dimensionless nonlinear coupled flow equations of the present mathematical model are numerically solved, taking into consideration the proper initial and boundary conditions, using the explicit Finite Difference (FTCS) method. The numerical technique's stability is depending on the selection of the time step (Δt) and grid size (Δx). A value of $\Delta t = 0.00001$ and $\Delta x = 0.025$ has been selected to meet the stability requirements. Several earlier investigations [32-34] have demonstrated that these temporal and spatial increment levels are adequate to assure the convergence and stability of the FTCS approach. Additionally, it has been highlighted in Hoffmann's book [35] that these selections of Δt and Δx support the numerical scheme's robustness and convergence.

3.1. Numerical procedure

The steps necessary to determine the formulation of finite difference for each of the partial derivatives are outlined in this section.

$$\frac{\partial w}{\partial t} \cong \frac{(w)_j^{k+1} - (w)_j^k}{\Delta t}, \tag{33}$$

$$\frac{\partial w}{\partial x} \cong \frac{(w)_{j+1}^k - (w)_{j-1}^k}{2\Delta x} = w_x, \tag{34}$$

$$\frac{\partial^2 w}{\partial x^2} \cong \frac{(w)_{j+1}^k - 2(w)_j^k + (w)_{j-1}^k}{(\Delta x)^2} = w_{xx}. \tag{35}$$

3.2. Validation Code

In order to verify the finite difference solution that was calculated using the methods from the previous section, a validation of the velocity and temperature profiles was made with the outcomes of Shabbir et al. [36] and Eldesoky et al. [37], taking stenosis height (δ=0.1), without nanoparticles (ϕ=0.0), Newtonian fluid ($\beta \to \infty$), ignoring permeability ($k \to \infty$), without magnetic field (M=0) and disregarding thermal radiation ($R_d = 0$) . It is observed that both of the solutions exhibit great agreement as shown in Figure 3 (a)-(b). Furthermore, this attests to the accuracy of the finite difference calculation that is then used for all graphical results.

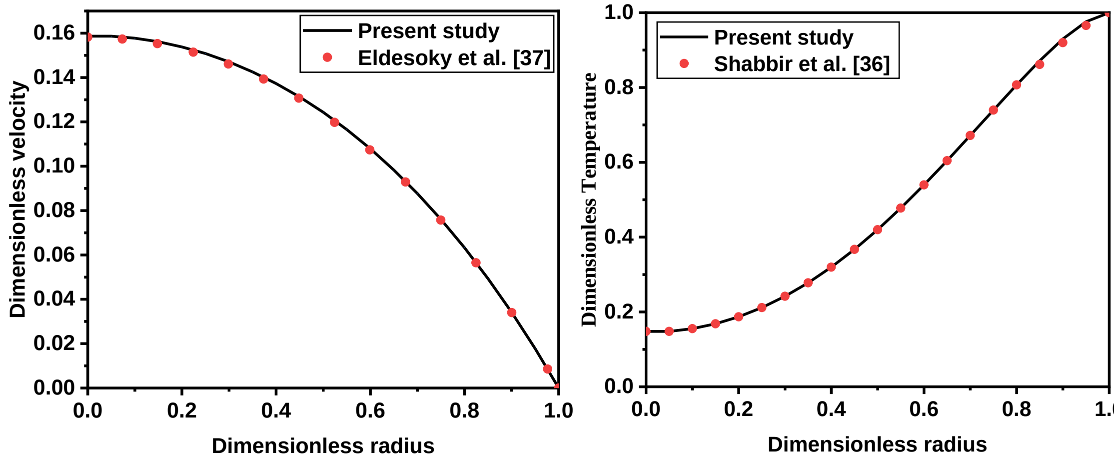

(a) (b)

Fig 3: Comparison results for (a) dimensionless velocity profile (b) dimensionless temperature profile

4. Results and discussion

This part presents the hemodynamic properties of an artery containing gold nanoparticles and two distinct stenoses. Graphical findings for several flow parameters, notably flow velocity, temperature distribution, WSS, flow rate, and flow resistance, are shown in Figures. These graphs provide a comparison of the hemodynamic properties in the stenotic area for the two types of arterial constriction (composite and irregular). The thermophysical amounts of gold nanoparticles (Au) and blood (base fluid) are shown in Table 1, while Table 2 displays the default values for the parameters used in the simulation.

Table 1: Base fluid and nanoparticles thermophysical properties [30].

Physical properties	Fluid phase (*f*) (Blood)	Solid nanoparticle phase (S)
ρ (kg/m^3)	1063	19320
k (W/m.K)	0.492	314
Cp (J / kg. K)	3594	129
γ (1/k)$\times 10^{-5}$	0.18	1.67
σ (S / m)	0.667	45×10^6

Table 2: Default entry parameter values.

δ	ϕ	β	Pr	Re	Br	Ma	k	α	B_1	B_2	Gr
0.1	0.03	2	15	1	2	0.5	0.3	$\pi/3$	1.14	0.5	0.1

4.1. Axial velocity

Figures 4 show the velocity profiles for various values of (a) Casson fluid parameter β, (b) nanoparticles volume fraction ϕ, (c) magnetic parameter Ma. The Casson parameter is related to the non-Newtonian Casson fluid nature and changes inversely with the yield stress. Consequently, increasing β causes the fluid's yield stress to decrease, this decrease in the yield stress means the internal structural forces holding the Casson fluid together are becoming weaker causing the fluid to relax and flow more rapidly as shown in Figure 4-(a). Figure 4-(b) shows that the axial blood flow accelerates as the concentration of nanoparticles increases, resulting in an increased velocity profile. The results presented are also supported by the study conducted by Tripathi et al. [38], which investigated blood flow through an inclined artery with stenosis. By decreasing the blood's viscosity and enhancing its ability to pass through the constricted artery, this can actually aid to improve the blood's velocity. Nanomaterials may be able to enhance blood flow velocity in atherosclerotic arteries by means of mechanical support and targeted medication administration. Additionally, they increase the circulation of oxygen-rich blood to organs, which lowers the likelihood of blockages. A decrease in the velocity profile is observed in Figure 4-(c) due to Lorentz force that restricted blood which created by the applied magnetic field. The Lorentz force acts on the charged particles in the blood, including the ions and electrons. This force creates a drag on the motion of the blood, decreasing its overall velocity. The stronger the magnetic field, the greater the Lorentz force and the more significant the reduction in blood flow velocity. Thus, the magnetic field performs a major role in the dynamics of blood flow in the arteries. As a result, it can be a useful tool in the identification and management of several cardiovascular conditions. Static magnetic fields are used in MRI to create detailed images of internal body structures. On the other hand, because the reduction of the blood velocity allows platelets and other clotting components to collect, it may potentially increase the risk of thrombosis. Furthermore, the axial velocity of the composite stenosis is much higher than that of the irregular one, as these figures demonstrate.

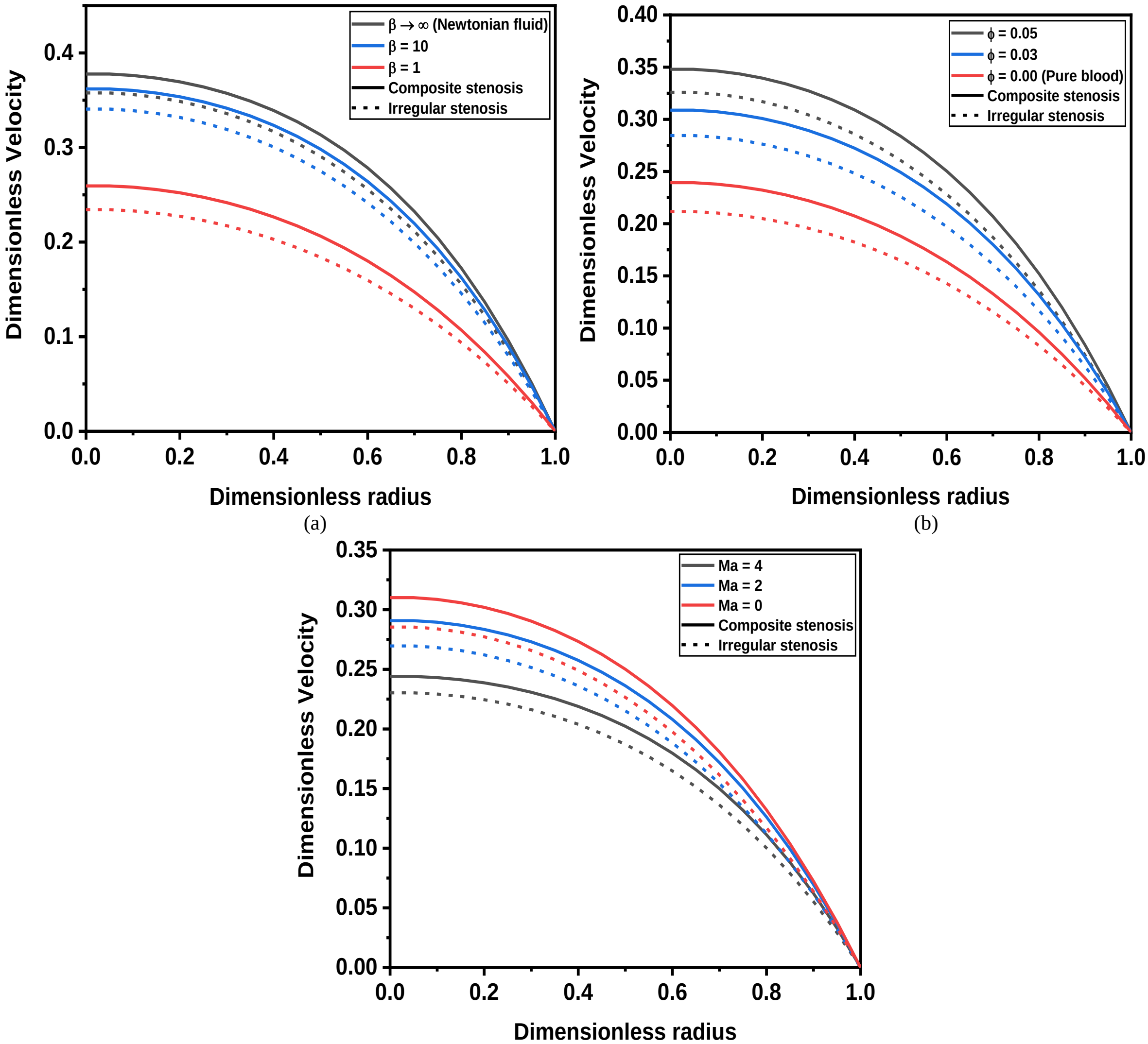

(c)

Fig 4: Effect of (a) Casson parameter β (b) Nanoparticle volume fraction (c) Magnetic parameter on velocity profile

4.2. Temperature profile

Figure 5 depicts the influence of (a) nanoparticle volume fraction ϕ (b) Brinkman number Br (c) parameter of thermal radiation R_d on the temperature profile. Figure 5-(a) describes that the temperature profile rises steadily as the volume fraction upsurges. As the concentration of nanoparticles increases, the overall surface area-to-volume ratio of the system grows, facilitating enhanced heat transfer. The larger surface area allows for more efficient dissipation and absorption of thermal energy, leading to a noticeable rise in the temperature. This validates the thermal enhancing capabilities of nanoparticles. Figure 5-(b) shows that the temperature is improved by increasing the Brinkman number values. The Brinkman number is the ratio of viscous heating to conductive heating. A higher Brinkman number results in less conductive heating. Since the Brinkman number describes the degree of dissipation effects, there is a direct correlation between increased blood temperature and the energy dissipation caused by fluid friction. It indicates that the viscous dissipation, or the heat generated due to the internal friction within the fluid, becomes more dominant compared to the conductive heat transfer. This means that more heat is being generated within the fluid itself, rather than being efficiently transferred to the surroundings. Due to the inverse relationship between R_d and thermal conductivity, the system appears to emit the most heat. Radiation generates thermal energy within the circulation; therefore, an increase in radiation exposure results in a temperature elevation of the body, as shown in Figure 5-(c), the phenomena can be explained physically by the heating of blood vessel walls due to the effects of radiation produced during therapy radiation. The blood temperature rises as a result in the area around the blood vessels. In order to provide more oxygen to tissues and muscles, vasodilation also happens during entrainment or other times when muscles are under constant stress. The interaction of free electrons within nanoparticles with right-wavelength light induces oscillations. The heat created by these oscillations permeates the encircling environment and eliminates malignant cells. There are numerous applications for this discovery in thermal therapy. Furthermore, irregular stenosis has a greater maximum temperature than composite stenosis. The geometric form of the stenosis affects the diffusion of heat and nanoparticles in the circulation.

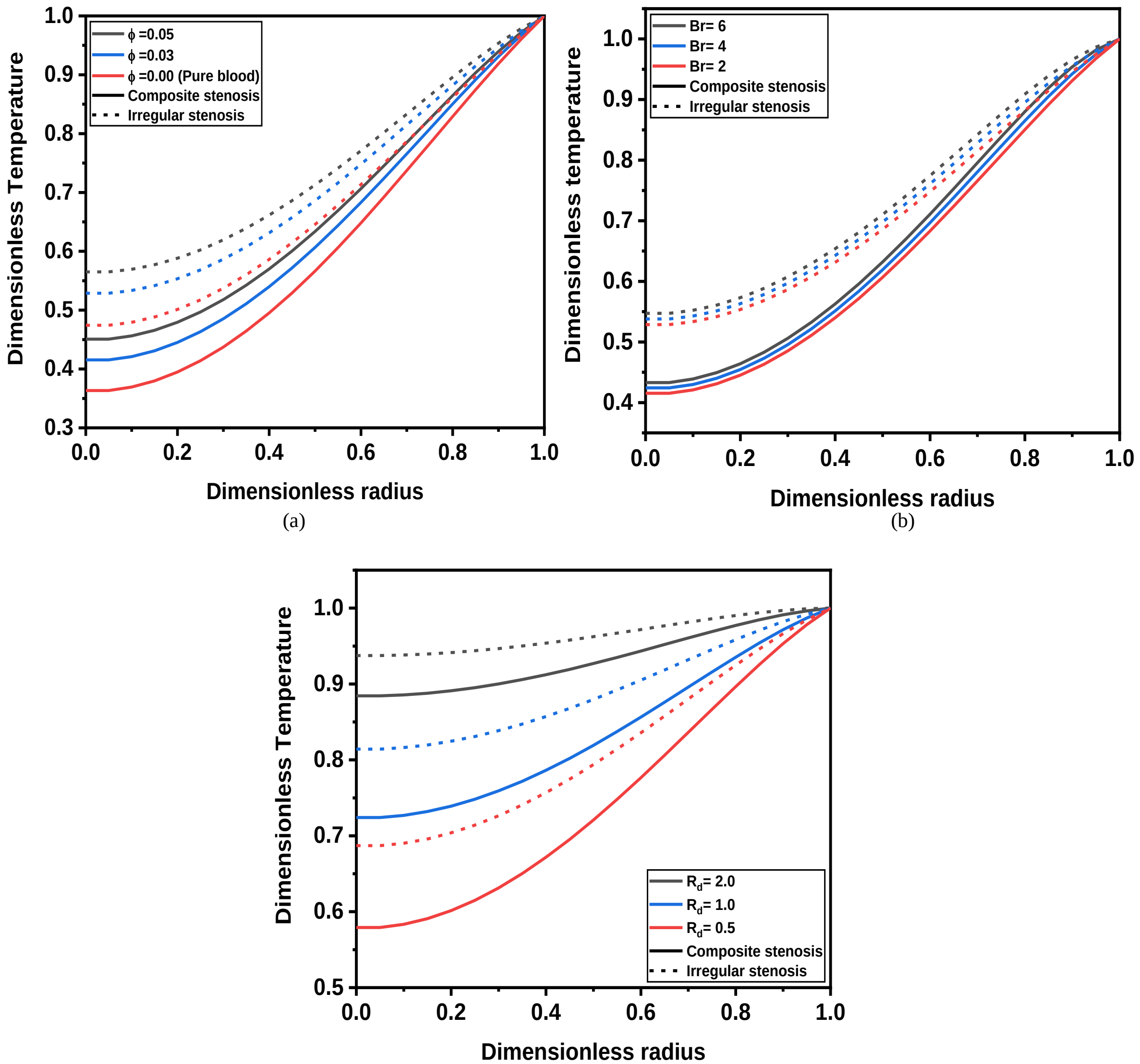

(c)

Fig 5: Effect of (a) Nanoparticle volume fraction (b) Brinkman number (c) thermal radiation on temperature profile

4.3. Flow rate, resistance to flow and wall shear stress

The effects of B_2 body acceleration on the flow rate profile for irregular and composite stenosis are shown in Figure 6-(a). The flow rate of the blood grows with body acceleration. This figure shows how the flow's periodic nature changes as the magnitude of the body's acceleration rises. This means that the rate of blood flow rises in a vibratory environment. During physical activity or movement, the body experiences acceleration, this directly impacts the flow rate of blood. As the body accelerates, the muscles require more oxygen and nutrients to sustain the increased energy demands. To meet this heightened need, the cardiovascular system responds by increasing the rate of blood flow. Because of this, some individuals could have headaches that make them throw up. A thorough examination of Figure 6-(b) shows that the effects of the magnetic field angle result in a greater wall shear stress, with a change in the inclination angle between $\alpha = 0$ and $\pi/2$. If the magnetic field is aligned perpendicular to the fluid flow, it can create a Lorentz force that acts on the charged particles within the fluid. This Lorentz force, perpendicular to the fluid flow, can alter the fluid motion. This decreased fluid motion can result in a lower wall shear stress. Conversely, if the magnetic field is aligned parallel to the fluid flow, the Lorentz force will be minimized, and the impact on the wall shear stress will be more pronounced as the fluid interacts more forcefully with the surface without the additional influence of the magnetic field. Dimensionless resistance to flow for various values of porous media permeability k and stenosis height is shown in Figure 6-(c). This graphic show that an increase in the porous medium's permeability k causes the resistance to flow amplitude to decrease, the resistance to flow diminishes, implying that flow is greatly increased. In another word, an increase in permeability amplitude led to a drop in the Darcian drag force's magnitude, which in turn increased flow. Furthermore, as $k \to \infty$, this impact becomes less significant. This figure also show the stenotic region for two distinct stenosis forms and stenosis height δ values. It illustrates how the arterial blockage that prevents blood flow causes the resistance to flow to increase as δ rises. When stenosis gets severe, the artery narrows significantly, decreasing the volume of blood that can pass via artery. This decrease in the section zone of the vessel limits the volume of blood that may flow within the artery, resulting in a drop in the velocity of blood flow and the possibility of various issues.

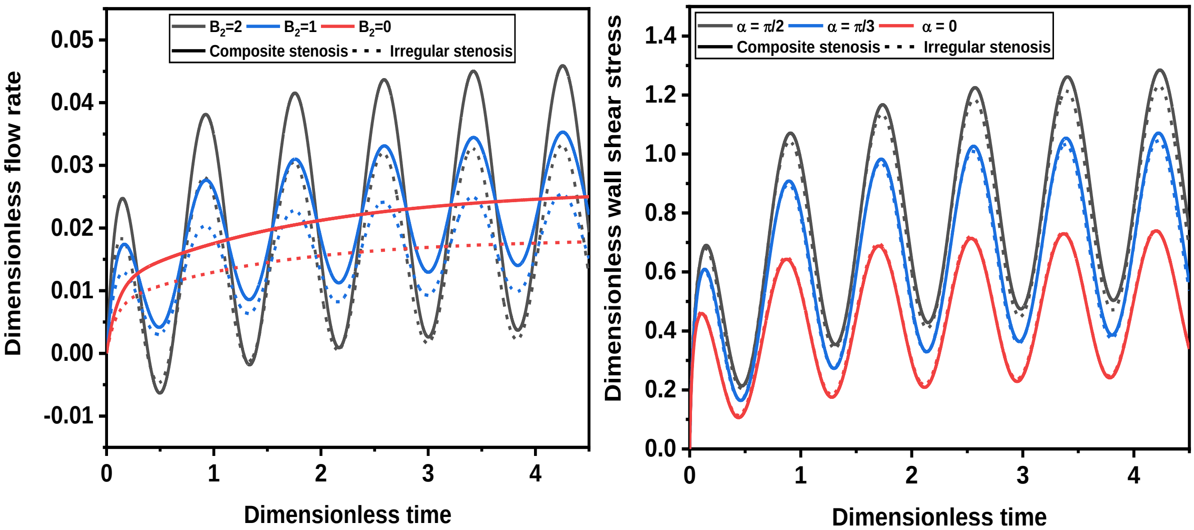

(a) (b)

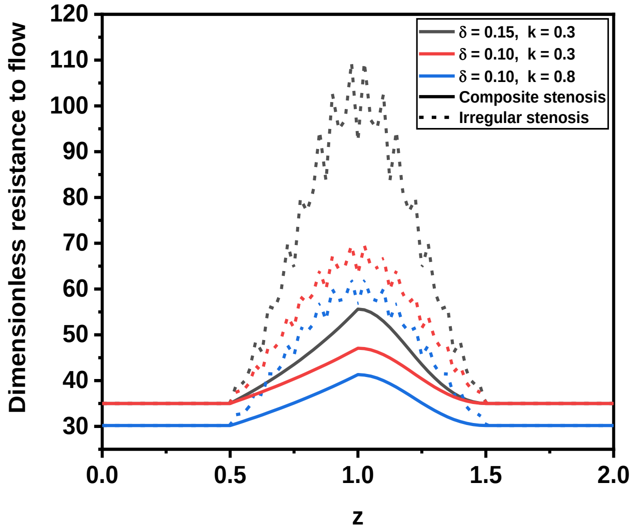

(C)

Fig 6: (a) Impact of parameter of body acceleration B_2 on flow rate (b) Impact of inclination angle of magnetic field α on wall shear stress (c) Impact of stenosis severity and permeability parameter k on resistance to flow

5. Conclusion

A numerical study was conducted on the transient flow of blood via stenosis artery under an inclined magnetic field with the addition of gold nanoparticles, and comparing two stenosis shapes. Thermal radiation and viscous dissipation was also considered. To represent blood rheology, the Casson model was employed. For more realistic flow circumstances, a pulsatile pressure gradient is included with periodic body acceleration. A method of finite difference was applied for the resolution of the partial differential equations of the problem.

The main conclusions of the current study are cited below:

- Increasing the volume fraction of nanoparticles leads to a rise in temperature and velocity profiles.
- External magnetic fields reduce the velocity profile substantially while the increase of the angle of inclination of magnetic field increases the wall shear stress.
- Resistance to flow increases with increasing stenosis height and decreases permeability parameter.
- Composite stenosis shows better results for velocity profile while the opposite is observed for the temperature profile.

Acknowledgements

Not applicable

References

[1] Y. Jiang, C. Reynolds, C. Xiao, W. Feng, Z. Zhou, W. Rodriguez, S. C. Tyagi, J. W. Eaton, J. T. Saari, Y. J. Kang, Dietary copper supplementation reverses hypertrophic cardiomyopathy induced by chronic pressure overload in mice, *J Exp Med*, Vol. 204, No. 3, pp. 657-66, Mar 19, 2007.

[2] S. Ijaz, S. Nadeem, Slip examination on the wall of tapered stenosed artery with emerging application of nanoparticles, *International Journal of Thermal Sciences*, Vol. 109, pp. 401-412, 2016.

[3] B. Bahrami, M. Hojjat-Farsangi, H. Mohammadi, E. Anvari, G. Ghalamfarsa, M. Yousefi, F. Jadidi-Niaragh, Nanoparticles and targeted drug delivery in cancer therapy, *Immunol Lett*, Vol. 190, pp. 64-83, Oct, 2017.

[4] R. Gandhi, B. K. Sharma, Q. M. Al-Mdallal, H. V. R. Mittal, Entropy generation and shape effects analysis of hybrid nanoparticles (Cu-Al2O3/blood) mediated blood flow through a time-variant multi-stenotic artery, *International Journal of Thermofluids*, Vol. 18, No. December 2022, pp. 100336-100336, 2023.

[5] W. P. Walawender, T. Y. Chen, D. F. Cala, An approximate casson fluid model for tube flow of blood, *Biorheology*, Vol. 12, No. 2, pp. 111-119, 1975.

[6] Sarifuddin, S. Chakravarty, P. K. Mandal, Numerical simulation of casson fluid flow through differently shaped arterial stenoses, *Zeitschrift fur Angewandte Mathematik und Physik*, Vol. 65, No. 4, pp. 767-782, 2014.

[7] P. Das, Sarifuddin, J. Rana, P. K. Mandal, Solute dispersion in transient Casson fluid flow through stenotic tube with exchange between phases, *Physics of Fluids*, Vol. 33, No. 6, 2021.

[8] R. Padma, R. T. Selvi, R. Ponalagusamy, Electromagnetic control of non-Newtonian fluid (blood) suspended with magnetic nanoparticles in the tapered constricted inclined tube, *AIP Conference Proceedings*, Vol. 2336, 2021.

[9] R. Gandhi, B. K. Sharma, O. D. Makinde, Entropy analysis for MHD blood flow of hybrid nanoparticles (Au–Al2O3/blood) of different shapes through an irregular stenosed permeable walled artery under periodic body acceleration: Hemodynamical applications, *ZAMM - Journal of Applied Mathematics and Mechanics / Zeitschrift für Angewandte Mathematik und Mechanik*, Vol. n/a, No. n/a, pp. e202100532-e202100532, 2022.

[10] C. S. K. Raju, H. T. Basha, N. F. M. Noor, N. A. Shah, S.-J. Yook, Significance of body acceleration and gold nanoparticles through blood flow in an uneven/composite inclined stenosis artery: A finite difference computation, *Mathematics and Computers in Simulation*, Vol. 215, pp. 399-419, 2024.

[11] J. Tripathi, B. Vasu, O. A. Bég, B. R. Mounika, R. S. R. Gorla, Numerical simulation of the transport of nanoparticles as drug carriers in hydromagnetic blood flow through a diseased artery with vessel wall permeability and rheological effects, *Microvascular Research*, Vol. 139, No. August 2021, 2022.

[12] A. Ali, S. Das, Applications of neuro-computing and fractional calculus to blood streaming conveying modified trihybrid nanoparticles with interfacial nanolayer aspect inside a diseased ciliated artery under electroosmotic and Lorentz forces, *International Communications in Heat and Mass Transfer*, Vol. 152, pp. 107313-107313, 2024.

[13] I. E. Glili, M. Driouich, Pulsatile flow of EMHD non-Newtonian nano-blood through an inclined tapered porous artery with combination of stenosis and aneurysm under body acceleration and slip effects and aneurysm under body acceleration and slip effects, *Numerical Heat Transfer, Part A: Applications*, Vol. 0, No. 0, pp. 1-29, 2024.

[14] I. El Glili, M. Driouich, Impact of inclined magnetic field on non-orthogonal stagnation point flow of CNT-water through stretching surface in a porous medium, *Journal of Thermal Engineering*, Vol. 10, No. 1, pp. 115-129, 2024.

[15] S. Dolui, B. Bhaumik, S. De, Combined effect of induced magnetic field and thermal radiation on ternary hybrid nanofluid flow through an inclined catheterized artery with multiple stenosis, *Chemical Physics Letters*, Vol. 811, pp. 140209-140209, 2023.

[16] I. El Glili, M. Driouich, The Effect of Nonlinear Thermal Radiation on EMHD Casson Nanofluid over a Stretchable Riga Plate with Temperature-Dependent Viscosity and Chemical Reaction, *Physical Chemistry Research*, Vol. 12, No. 1, pp. 157-173, 2024. en

[17] R. Gandhi, B. K. Sharma, N. K. Mishra, Q. M. Al-Mdallal, Computer Simulations of EMHD Casson Nanofluid Flow of Blood through an Irregular Stenotic Permeable Artery: Application of Koo-Kleinstreuer-Li Correlations, *Nanomaterials*, Vol. 13, No. 4, 2023.

[18] B. K. Sharma, R. Gandhi, T. Abbas, Magnetohydrodynamics hemodynamics hybrid nanofluid flow through inclined stenotic artery ∗, Vol. 44, No. 3, pp. 459-476, 2023.

[19] A. C. Burton, Physiology and Biophysics of the Circulation: An Introductory Text, 1965, pp. 394-394.

[20] A. Zaman, H. H. Khan, A. A. Khan, F. u. Shah, Body acceleration effects on two-directional unsteady Cross fluid (blood) flow in time variant stenosed (w-shape) artery, *Chinese Journal of Physics*, Vol. 86, pp. 136-147, 2023.

[21] A. Daiz, A. Bahlaoui, I. Arroub, S. Belhouideg, A. Raji, M. Hasnaoui, Modeling of nanofluid mixed convection within discretely heated lid-driven inclined cavity using lattice Boltzmann method, *AIP Conference Proceedings*, Vol. 2761, No. 1, pp. 40018-40018, 2023.

[22] Y. Foukhari, M. Sammouda, M. Driouich, MHD natural convection in an annular space between two coaxial cylinders partially filled with metal base porous layer saturated by Cu–water nanofluid and subjected to a heat flux, *Journal of Thermal Analysis and Calorimetry*, 2023.

[23] Y. Ighris, Y. Bouhouchi, Y. Elguennouni, J. Baliti, M. Hssikou, A. Boumezzough, Numerical study of natural convection in an inclined cavity filled with Al2O3/Cu-H2O nanofluids, *Numerical Heat Transfer, Part A: Applications*, pp. 1-25.

[24] I. A. Abbas, Generalized thermoelastic interaction in functional graded material with fractional order three-phase lag heat transfer, *Journal of Central South University*, Vol. 22, No. 5, pp. 1606-1613, 2015.

[25] T. Saeed, I. Abbas, Finite element analyses of nonlinear DPL bioheat model in spherical tissues using experimental data, *Mechanics Based Design of Structures and Machines*, Vol. 50, No. 4, pp. 1287-1297, 2022.

[26] A. D. Hobiny, I. A. Abbas, Nonlinear analysis of dual-phase lag bio-heat model in living tissues induced by laser irradiation, *Journal of Thermal Stresses*, Vol. 43, No. 4, pp. 503-511, 2020.

[27] M. Marin, A. Hobiny, I. Abbas, Finite element analysis of nonlinear bioheat model in skin tissue due to external thermal sources, *Mathematics*, Vol. 9, No. 13, pp. 1-9, 2021.

[28] I. Abbas, A. Hobiny, H. Alshehri, S. Vlase, M. Marin, Analysis of Thermoelastic Interaction in a Polymeric Orthotropic Medium Using the Finite Element Method, *Polymers*, Vol. 14, No. 10, pp. 1-12, 2022.

[29] I. El Glili, A. Saidi, Y. Foukhari, M. Driouich, M. Sammouda, Numerical simulation of unsteady blood based Carreau nanofluid flow in an inclined porous saturated artery having overlapping stenosis with electro-osmosis, *Numerical Heat Transfer; Part A: Applications*, Vol. 0, No. 0, pp. 1-31, 2024.

[30] I. El Glili, M. Driouich, Computational study of the pulsatile EMHD Sutterby nanofluid flow of blood through an inclined tapered porous artery having overlapping stenosis with body acceleration, *Archive of Applied Mechanics*, 2024.

[31] J. Tripathi, B. Vasu, O. A. Bég, Computational simulations of hybrid mediated nano- hemodynamics (Ag-Au/Blood) through an irregular symmetric stenosis, *Computers in Biology and Medicine*, Vol. 130, pp. 104213-104213, 2021.

[32] A. Zaman, N. Ali, M. Sajid, Numerical simulation of pulsatile flow of blood in a porous-saturated overlapping stenosed artery, *Mathematics and Computers in Simulation*, Vol. 134, pp. 1-16, 2017.

[33] A. Zaman, N. Ali, O. Anwar Bég, Numerical simulation of unsteady micropolar hemodynamics in a tapered catheterized artery with a combination of stenosis and aneurysm, *Medical and Biological Engineering and Computing*, Vol. 54, No. 9, pp. 1423-1436, 2016.

[34] M. Fahim, M. Sajid, N. Ali, Non-isothermal flow of Sisko fluid in a stenotic tube induced via pulsatile pressure gradient and periodic body acceleration, *Physica Scripta*, Vol. 96, No. 8, 2021.

[35] K. Hoffmann, S. Chiang, Computational Fluid Dynamics. Vol. 1, pp. p.486-p.486.

[36] M. S. Shabbir, Z. Abbas, N. Ali, Numerical study of heat and mass transfer on the pulsatile flow of blood under atherosclerotic condition, *International Journal of Nonlinear Sciences and Numerical Simulation*, 2022.

[37] I. M. Eldesoky, M. H. Kamel, R. M. Hussien, R. M. Abumandour, Numerical Study of Unsteady MHD Pulsatile Flow through Porous Medium in an Artery Using Generalized Differential Quadrature Method (GDQM), *International Journal of Materials, Mechanics and Manufacturing*, Vol. 1, No. 2, pp. 200-206, 2013.

[38] J. Tripathi, B. Vasu, O. A. Bég, R. S. R. Gorla, P. K. Kameswaran, Computational simulation of rheological blood flow containing hybrid nanoparticles in an inclined catheterized artery with stenotic, aneurysmal and slip effects, *Computers in Biology and Medicine*, Vol. 139, No. October, 2021.